ACS OMEGA

Open Access

http://pubs.acs.org/journal/acsodf

Article

Yttrium-Modified $B_{12}N_{12}$ Nanocages for High-Performance H_2 Sensing: Insights from DFT Calculations on Sensitivity, Selectivity, and Recovery

Wellington da Conceição Lobato do Nascimento, Natanael de Sousa Sousa, Adilson Luís Pereira Silva,* and Adeilton Pereira Maciel

Cite This: https://doi.org/10.1021/acsomega.5c11273

Read Online

ACCESS | Metrics & More | Article Recommendations | Supporting Information

ABSTRACT: Boron nitride ($B_{12}N_{12}$) nanocages have attracted considerable attention due to their exceptional structural stability and tunable electronic properties, making them promising candidates for gas-sensing applications. In this study, DFT-D3 calculations at the B3LYP/def2-TZVP level, including relativistic effects for yttrium (SARC-ZORA-def2-TZVP), were employed to investigate H_2 adsorption on pristine and Y-modified (doped, decorated, and encapsulated) $B_{12}N_{12}$ nanocages. The pristine nanocage exhibited weak physisorption (E_{ads} = −0.04 eV), whereas the Y@b_{64} configuration demonstrated strong chemisorption (E_{ads} = −0.96 eV), pronounced electronic sensitivity (ΔE_{gap} = 74.94%), and a feasible recovery time (τ = 166.8 s). Analyses of electrostatic potential, molecular dynamics (1000 ps), IR, and UV−vis spectra confirmed the structural robustness and optical detectability of H_2. Furthermore, the Y@b_{64} nanocage showed remarkable selectivity toward H_2 compared to common interfering gases (CH_4, CO, H_2S, and N_2). Overall, Y@b_{64} combines high adsorption energy, strong sensitivity, and efficient recovery time, underscoring its potential as a selective, stable, and high-performance H_2 gas sensor.

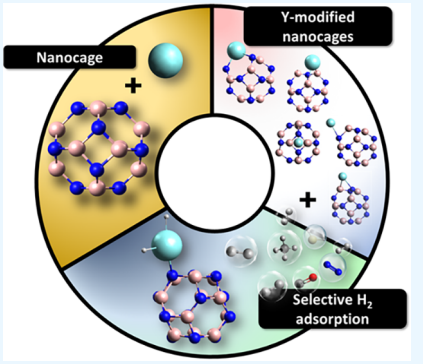

1. INTRODUCTION

The development of sensors for odorless, colorless, and toxic gases such as H_2, NH_3, SO_2, O_2, NO_2, H_2S, CO, and CO_2 has generated great interest in the scientific community and industry.[1−3] Sensors capable of quickly and accurately identifying these gases play a crucial role in mitigating environmental impacts, such as global warming, and in advancing alternative energy sources. In the case of hydrogen (H_2), efficient sensors are essential to ensure safety and efficiency in industrial processes such as coal mining, nuclear reactors, and semiconductor manufacturing, where rigorous monitoring is required to reduce risks and optimize operations.[4−7]

Nanomaterials, including nanosheets, nanotubes, and nanocages, have been widely studied as gas sensors due to their exceptional electronic properties and high surface area.[8] Among them, boron nitride-based structures stand out, such as nanotubes (BNNTs), two-dimensional structures (h-BN), nanoclusters (B_6N_6), and nanocages $(BN)_n$, combining sensitivity, rapid detection, and short recovery times. Theoretical studies using DFT calculations have demonstrated the efficiency of these systems in the adsorption of various gases. For example: Aasi et al.[9] observed that Pt- and Pd-decorated novel green phosphorene exhibit high reactivity for C_2H_2, H_2, and CH_4; Kalateh et al.[10] showed that $B_{16}N_{16}$ has superior electronic adsorption properties for H_2 compared to C_{32} and B_8C_{24}; and Choir et al.[11] found that $B_{12}N_{12}$ nanocages interact spontaneously and exothermically with CO_2 and H_2 (E_{ads} = −26.86 and −6.94 kJ/mol, respectively). Nair et al.[12] also demonstrated that $B_{12}N_{12}$ strongly adsorbs gases such as AsH_3, H_2Se and H_2S, while H_2 and CH_4 present weaker interactions, with relevant modifications in reactivity indices, such as chemical potential and hardness.

Despite the potential of $B_{12}N_{12}$ for atmospheric gas sensors, some molecules such as H_2, H_2S, CO, $COCl_2$, and NO do not spontaneously adsorb on the pure cage due to weak interactions, requiring structural modifications to optimize their electronic properties.[13−17] The insertion of transition metals is an efficient strategy to increase the affinity of the nanocage for different gases. Experimentally, Oku et al.[18−21] synthesized $B_{12}N_{12}$ and $B_{36}N_{36}$ cages, pure and modified with transition metals (Fe, Ag, La, and Y), confirming their structures by electron microscopy and mass spectrometry. Yttrium, in particular, proved effective in improving H_2 adsorption, for example: (i) Wang and Tian[22] indicated, via DFT, that each Y atom in a $C_{48}B_{12}$ cage can bind up to six H_2 molecules with significant binding energies,

Received: October 27, 2025
Revised: December 21, 2025
Accepted: December 29, 2025

suggesting chemisorption-type interactions; (ii) Kundu and Chakraborty[23] showed, via DFT, that Y atom attached on Triazine can adsorb seven H_2 molecules with binding energy of 0.33 eV/H_2 leading to 7.3 wt % of H_2; (iii) Srivastava et al.[24] reported experimentally that the chemoresistive gas sensor based on Y-CeO exhibited excellent long-term stability, outstanding sensitivity, fast response and recovery times, and selectivity to H_2 in comparison to other gases. Revealing the exceptional potential of the Y-CeO sensor as a low-trace H_2 gas detector; (iv) Ferlazzo et al.[25] showed experimentally that the novel yttria-doped ZrO_2 exhibited excellent characteristics in terms of sensor response, fast response and recovery time (5 and 10 s, respectively) and good selectivity to H_2.

Therefore, all of these findings motivated us to design a system that efficiently binds the H_2 gas by structural modification of $B_{12}N_{12}$ nanocage with Y metal and helps in detecting this gas in the environment. The novelty of this work lies in the comprehensive comparative analysis of five distinct yttrium-based configurations, offering a deeper understanding of the electronic and structural factors that govern the interaction between H_2 molecules and the nanocage surface.

This study aims to fill this gap by employing density functional theory (DFT) calculations, including relativistic effects, to elucidate how different yttrium insertion strategies influence the adsorption behavior of H_2. By mapping these effects, we identify key mechanisms that enhance selectivity, sensitivity, and adsorption efficiency, ultimately contributing to the rational design of high-performance hydrogen sensors. In this context, our investigation aims to identify a material with the potential to be applied as a selective sensor, exhibiting high sensitivity and rapid detection of hydrogen gas in the environment.

2. COMPUTATIONAL METHODOLOGY

Density Functional Theory (DFT) calculations were performed using ORCA 5.0.[26] The isolated and yttrium-modified $B_{12}N_{12}$ nanocages were optimized with the B3LYP functional and Grimme D3 dispersion correction,[27,28] suitable for long-range interactions. The B3LYP-D3 functional was adopted due to its accuracy in geometries and vibrational frequencies, combined with low computational cost. Thus, B3LYP stands out as a stable, economical and reproducible option, as validated in gas adsorption studies.[29,30] Different basis sets were used: def2 with relativistic effects SARC-ZORA-def2-TZVP for yttrium and ZORA-def2-TZVP for the other elements. The adopted convergence criteria were: RMS gradient (5×10^{-6} Hartree), RMS shift (1×10^{-4} Hartree/Bohr), maximum gradient (2×10^{-3} Bohr), maximum shift (3×10^{-4} Hartree/Bohr) and energy (4×10^{-3} Hartree). Frequency analyses confirmed the global minima of the optimized structures. The structural modification of $B_{12}N_{12}$ with yttrium gave rise to five distinct structures:[13,31]

- Y-doped ($YB_{11}N_{12}$), in which one B atom of $B_{12}N_{12}$ is replaced by a Y atom;
- Y-doped ($YB_{12}N_{11}$), in which one N atom of $B_{12}N_{12}$ is replaced by a Y atom;
- Y-decorated (Y@b_{64}), in which a Y atom is externally adsorbed onto the $B_{12}N_{12}$ nanocage, positioned above one b_{64} bond that connects a hexagonal and a tetragonal ring;
- Y-decorated (Y@b_{66}), in which a Y atom is externally adsorbed onto the $B_{12}N_{12}$ nanocage, positioned above one b_{66} bond that connects two hexagonal rings;
- Y-encapsulated (Y@$B_{12}N_{12}$), where a Y is located inside the $B_{12}N_{12}$ nanocage.

The nanocages were optimized in their neutral forms (charge = 0). Preliminary spin-state tests showed that $B_{12}N_{12}$, $YB_{11}N_{12}$, and $B_{12}N_{11}Y$ converge to closed-shell singlet states (multiplicity = 1), confirming their diamagnetic character (see Table S1 in Supporting Information). In contrast, the Y-decorated and -encapsulated structures (Y@b_{64}, Y@b_{66}, and Y@$B_{12}N_{12}$) exhibit open-shell doublet ground states (multiplicity = 2), as evidenced by the distinct α/β orbital energies (Tables 1 and 3)

Table 1. Calculated Values of Formation Energy (E_{form}), Cohesive Energy (E_{coh}), Dipole Moment (DM), NPA Charge on the Y Atom (Q_{Metal}), Energy Gap (E_{gap}) and Work Function (Φ) for Isolated Systems

system	E_{form} (eV)	E_{coh} (eV)	DM (Debye)	Q_{Metal} (el)	E_{gap} (eV)	Φ (eV)
$B_{12}N_{12}$	−3.04	−7.33	0.00		6.80	4.46
$YB_{11}N_{12}$	−2.96	−7.25	9.75	2.024	3.72	4.70
$B_{12}N_{11}Y$	−2.91	−6.93	8.89	1.310	2.54	3.83
Y@b_{64}	−2.92	−7.07	5.90	1.134	2.43[a] 2.93[b]	3.14
Y@b_{66}	−2.91	−6.99	5.64	0.986	2.30[a] 1.64[b]	3.72
Y@$B_{12}N_{12}$	−2.58	−6.71	1.79	0.576	2.07[a] 2.33[b]	3.41

[a]Spin up. [b]Spin down.

and a total spin population of 1.0, indicating the presence of one unpaired electron. After H_2 adsorption, all complexes retain the multiplicity of their corresponding ground states, showing that the magnetic behavior induced by yttrium remains unchanged upon interaction with the adsorbates. The stability of the systems was evaluated by determining the cohesive energy (E_{coh}) following eq 1[32]

$$E_{coh} = \frac{1}{N}(E_{nanocage} - xE_B - yE_N - zE_Y) \quad (1)$$

in this equation, $E_{nanocage}$ represents the total energy of the nanocage, whether pure or modified with yttrium. E_B, E_N, and E_Y correspond to the energies of the boron, nitrogen, and yttrium atoms. The variables x, y, and z denote the number of B, N, and Y atoms in the structure, while N represents the total number of atoms of the studied nanocages.

For thermodynamic analysis of the most viable systems to be synthesized and to compare with the cohesion energy data, we also calculated the formation energy of the nanocages, according to eq 2[33]

$$E_{form} = \frac{(E_{modified} - a\overline{E}_B - b\overline{E}_N - c\overline{E}_Y)}{N} \quad (2)$$

where the $E_{modified}$ is the total energy nanocage modified, $\overline{E}_B$, $\overline{E}_N$ and $\overline{E}_Y$ are the energies for elements in B_2, N_2 and cluster of the Y atom, respectively; a, b, and c are the numbers of B, N, and Y atoms, respectively, and N is the total number of atoms.

The energy gap E_{gap} is defined as the difference between the energy levels LUMO (E_{LUMO}) and HOMO (E_{HOMO}). The electronic sensitivity (ΔE_{gap}) of the interaction between the H_2/nanocages was determined using eq 2.[14]

https://doi.org/10.1021/acsomega.5c11273
ACS Omega XXXX, XXX, XXX−XXX

$$\Delta E_{gap} = \left[\frac{(E_{gap(nanocage\text{-}H_2)} - E_{gap(nanocage)})}{E_{gap(nanocage)}} \right] \times 100 \quad (3)$$

the $E_{gap(nanocage\text{-}H_2)}$ represents the energy gap associated with the interaction of H_2 with both pure and modified $B_{12}N_{12}$ nanocages, while $E_{gap(nanocage)}$ refers to the energy gap of pure or Y-modified $B_{12}N_{12}$. To better understand the spontaneity of the cage/gas adsorption process, thermodynamic parameters were analyzed. Specifically, the variation in adsorption enthalpy (ΔH_{ads}) and free energy (ΔG_{ads}) using eqs 4 and 5.[11]

$$\Delta G_{ads} = G_{gas\text{-}nanocage} - (G_{gas} + G_{nanocage}) \quad (4)$$

$$\Delta H_{ads} = H_{gas\text{-}nanocage} - (H_{gas} + H_{nanocage}) \quad (5)$$

$G_{gas\text{-}nanocage}$ and $H_{gas\text{-}nanocage}$ represent the free energy and enthalpy of gas-nanocage adsorption. H_{gas} and G_{gas} are related to the energies of H_2 gas and $G_{nanocage}$ and $H_{nanocage}$ are the energies of the isolated nanocages, respectively. Equation 5 was used to obtain adsorption energy (E_{ads}) values to study the interaction between $B_{12}N_{12}$ or yttrium-modified nanocages and H_2 gas.[16]

$$E_{ads} = E_{(nanocage\text{-}H_2)} - (E_{(nanocage)} + E_{(H_2)}) + E_{BSSE} \quad (6)$$

the system energy $E_{(nanocage\text{-}H_2)}$ corresponds to the $B_{12}N_{12}$ or Y–$B_{12}N_{12}$ nanocage with H_2, including the zero-point vibrational energy (ZPVE), while $E_{(nanocage)}$ and $E_{(H_2)}$ refer to the energies of the isolated nanocages and the H_2 molecule. The error correction of the basis set superposition (BSSE) was applied for greater accuracy in the interactions. The recovery time (τ) is given by eq 7[34−36]

$$\tau = v_0^{-1} e^{-E_{ads}/k_B T} \quad (7)$$

with $v_0 = 10^{12}$ s^{-1}, $k_B = 8.62 \times 10^{-5}$ eV K^{-1} and T is the thermodynamic temperature (K).[37] E_{ads} values between −0.3 and −1.0 eV result in τ of order of seconds,[38] indicating a sensor potential. The work function (Φ) was calculated from the frontier orbitals, and the variation ($\Delta\Phi$) before and after adsorption was the criterion for evaluating the applicability of the nanocages (eqs 8 and 9).

$$\Phi \approx E_H + \frac{1}{2}(E_L - E_H) \quad (8)$$

$$\Delta\Phi = \left| \frac{(\Phi_{(nanocage\text{-}H_2)} - \Phi_{(nanocage)})}{\Phi_{(nanocage)}} \times 100 \right| \quad (9)$$

where $\Phi_{(nanocage-H_2)}$ represents the work function values of the adsorbed systems ($B_{12}N_{12}/H_2$) and $\Phi_{(nanocage)}$ corresponds to the work function of the pure $B_{12}N_{12}$ or Y-modified nanocage. The quantum descriptor parameters were obtained based on the values of frontier orbitals (HOMO and LUMO)[39,40] by applying eqs 10−15.

$$IP \approx -E_{HOMO} \quad (10)$$

$$eA \approx -E_{LUMO} \quad (11)$$

$$\eta \approx \frac{1}{2}(E_{LUMO} - E_{HOMO}) \quad (12)$$

$$\mu \approx \frac{1}{2}(E_{LUMO} + E_{HOMO}) \quad (13)$$

$$S \approx \frac{1}{2\eta} \quad (14)$$

$$\omega = \frac{\mu^2}{2\eta} \quad (15)$$

The electrostatic potential map (MEP) and density of state spectra (DOS) were obtained using the MultiWfn program,[41] in addition to UV−vis spectra, in order to investigate the electronic and optical properties of the cage/gas interactions, elucidating the electronic distribution, reactivity and sensing potential toward H_2. The stability of the most favorable system after H_2 adsorption was evaluated by quantum molecular dynamics (MD) of 1000 ps, with an integration interval of 2 fs, using the GFN-1 Hamiltonian in the xTB software.[42]

The electrical conductivity (σ) can be employed to investigate the interactions of pure and modified $B_{12}N_{12}$ nanocages with H_2. Its value was calculated as eq 16[43,44]

$$\sigma = AT^{3/2} e^{(-E_{gap}/2k_B T)} \quad (16)$$

where A is a constant (electron m^{-3} K$^{-3/2}$), E_{gap} is the energy gap, k_B is the Boltzmann constant (8.62×10^{-5} eV K^{-1}) and T is the thermodynamic temperature (K). Based on this, the most promising yttrium-doped nanocage for H_2 detection was subjected to interactions with interfering gases (CH_4, CO, H_2S and N_2), with selectivity being analyzed by calculating the sensor response (S) and the selectivity coefficient (κ), according to eqs 17 and 18.[45,46]

$$S = \frac{|R_{gas} - R_{pure}|}{R_{pure}} = \frac{\left| \frac{1}{\sigma_{gas}} - \frac{1}{\sigma_{pure}} \right|}{\frac{1}{\sigma_{pure}}} = \frac{|\sigma_{pure} - \sigma_{gas}|}{\sigma_{gas}} \quad (17)$$

$$\kappa_{H_2-int} = \frac{S_{H_2}}{S_{int}} \quad (18)$$

the σ_{gas} represents the conductivity of the gas adsorbed, σ_{pure} is the conductance of the isolated nanocage and R_{gas} and R_{pure} represent the electrical resistance of the gas/cage system and pure nanocage, respectively. In eq 18, S_{H_2} and S_{int} indicate sensitivity to H_2 gas and to interferents gases, respectively, and κ_{H_2-int} represents the sensitivity ratio to H_2 against an interfering gas.

3. RESULTS AND DISCUSSION

3.1. Structural Analysis

The structure of the $B_{12}N_{12}$ nanocage was optimized, presenting a configuration with eight hexagonal and six tetragonal rings (Figure 1). In this geometry, all B and N vertices are equivalent. Two types of B−N bonds were identified: b_{64}, between hexagonal and tetragonal rings, with a length of 1.435 Å, and b_{66}, between hexagonal rings, with a length of 1.483 Å. These values are close to those reported by Zhao et al.,[47] who studied the structural and electronic properties of $B_{12}N_{12}$ doped with transition metals. For the tetragonal rings, the B−N−B and N−B−N angles were 80.5° and 98.9°, respectively, in agreement with the literature.[48−51]

The optimized structures of the pristine and yttrium-modified $B_{12}N_{12}$ nanocages ($YB_{11}N_{12}$, $B_{12}N_{11}Y$, Y@b_{64}, Y@b_{66}, and Y@$B_{12}N_{12}$) are shown in Figure 2. The replacement of B or N atoms by yttrium causes evident structural deformations, attributed to

https://doi.org/10.1021/acsomega.5c11273
ACS Omega XXXX, XXX, XXX−XXX

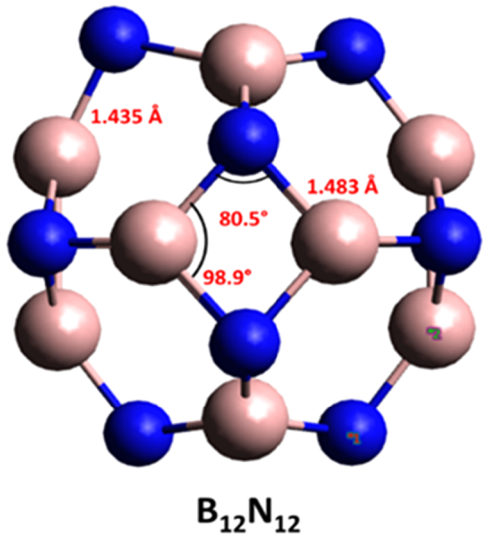

Figure 1. Optimized structure of $B_{12}N_{12}$ nanocage with B3LYP functional and ZORA-def2-TZVP basis set.

the larger atomic radius of Y compared to B and N. In the decorated structures, Y@b_{64} and Y@b_{66}, the B−N bond lengths near the metal increased to 2.460 Å and 2.380 Å, respectively, indicating significant local distortions. Similarly, the encapsulation in Y@$B_{12}N_{12}$ resulted in bond lengths of 2.620 Å (b_{66}) and 2.360 Å (b_{64}), greater than those of the pristine structure. These results demonstrate that yttrium modification, whether through doping, decoration, or encapsulation, induces structural changes in the $B_{12}N_{12}$ nanocage. The expansion of B−N bonds, in turn, directly affects electronic stability and molecular adsorption, aspects detailed in subsequent analyses. However, despite the structural changes, it is clear that all yttrium-modified structures are stable over 1000 ps, as shown by the molecular dynamics results.

In Table 1, we present the formation energy (E_{form}), cohesive energy (E_{coh}), dipole moment (DM), NPA charge on the Y atom (Q_{Metal}), energy gap (E_{gap}), and work function (Φ) for the pristine $B_{12}N_{12}$ and its yttrium-modified nanocages. The α-spin (spin up) and β-spin (spin down) orbital energies are reported for the open-shell systems. The pristine nanocage exhibited zero DM, while $YB_{11}N_{12}$ presented the highest value (9.75 D), and Y@$B_{12}N_{12}$ the lowest (1.79 D), reflecting a lower charge partitioning in the encapsulation.[52,53] These results are corroborated by the lower charges on the yttrium atom. The E_{coh} analysis indicates that the doped, decorated or encapsulated structures are less stable than the pristine $B_{12}N_{12}$, although $YB_{11}N_{12}$ stands out as the most stable among them (E_{coh} = −7.25 eV). In addition, the negative formation energy for all the nanocages confirms their thermodynamic stability.[54,55]

In this study, it was employed to investigate the interaction between the transition metal yttrium (Y) and the $B_{12}N_{12}$ nanocage, as presented in Table 1. The natural charges (NPA) indicate that Y acts as an electron donor, transferring electron density to the nanocage due to its lower electronegativity. Among the evaluated structures, the $YB_{11}N_{12}$-doped nanocage exhibited the highest charge transfer, demonstrating that substituting a boron atom with Y enhances electronic redistribution and directly influences the electronic and chemical properties of the nanocage. The work function (Φ) values, calculated by eq 8, were reduced after the modification with yttrium, except in $YB_{11}N_{12}$ (Φ = 4.70 eV), which maintained the highest value. The decorated system Y@b_{64} presented the lowest (Φ = 3.14 eV), evidencing the impact of the decoration on the electronic response.

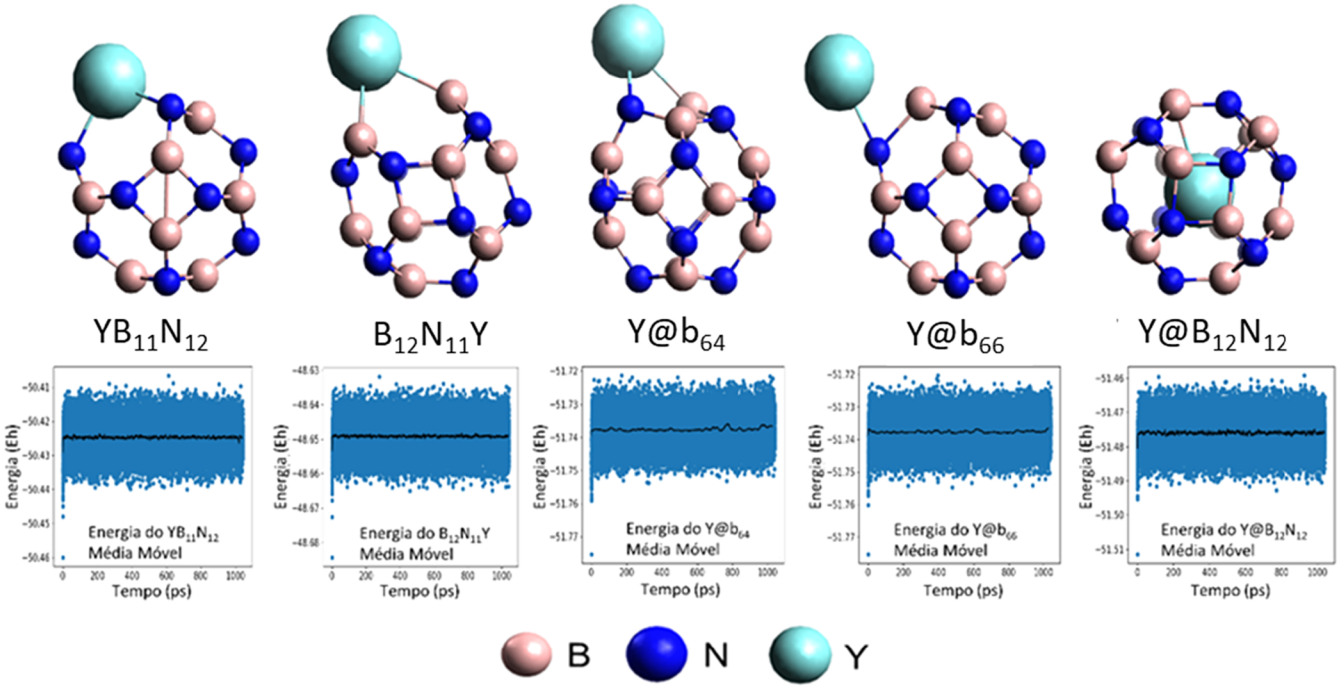

Figure 2. Illustration of the optimized structures and molecular dynamics of the $B_{12}N_{12}$ nanocage and the yttrium metal-modified nanocages: doped ($YB_{11}N_{12}$ and $B_{12}N_{11}Y$), decorated (Y@b_{64} and Y@b_{66}), and encapsulated (Y@$B_{12}N_{12}$).

https://doi.org/10.1021/acsomega.5c11273
ACS Omega XXXX, XXX, XXX−XXX

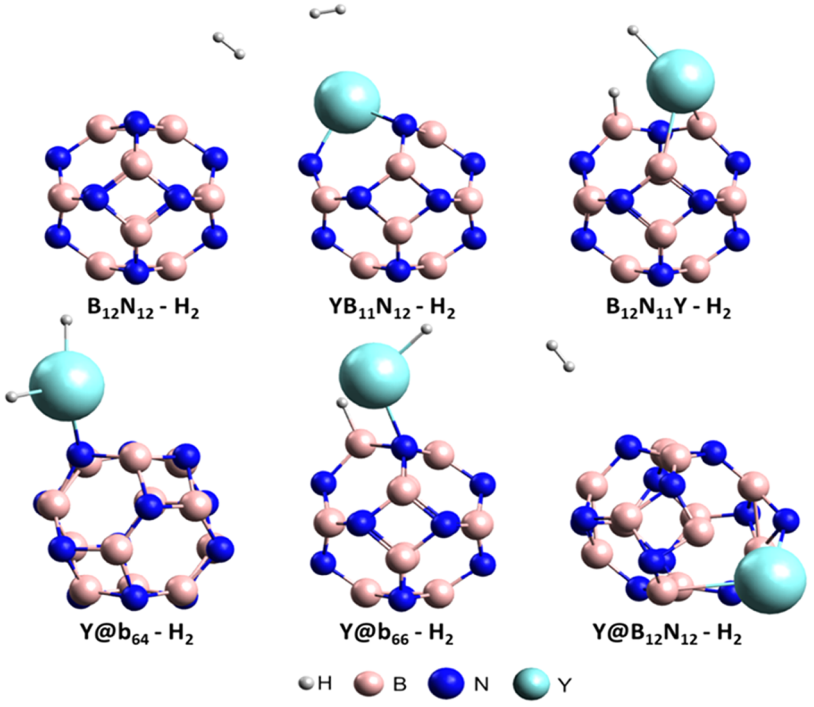

Figure 3. Optimized structures of hydrogen gas (H_2) adsorption on the surfaces of pure and Y-modified $B_{12}N_{12}$ nanocages.

3.2. Adsorption Analysis

Figure 3 shows the structures resulting from H_2 adsorption on the nanocages. Before locating the minimum-energy complexes, we explored different initial adsorption orientations. For the $B_{12}N_{12}$ and $Y@B_{12}N_{12}$ systems, we tested positions over B and N atoms. In the doped and decorated nanocages, H_2 was initially placed near the metal, allowing full geometric relaxation to reach the most stable configuration. Only a single initial position of H_2 was required for each system, as hydrogen is a small molecule that adjusts spontaneously during optimization. In the doped $B_{12}N_{11}Y{-}H_2$ and decorated $Y@b_{66}{-}H_2$ systems, H−H bond rupture and formation of new H−B and H−Y bonds were observed. In the $Y@b_{64}{-}H_2$ system, the H_2 molecule dissociated and bonded to the yttrium atom, giving rise to the H−Y−H configuration. This behavior was also reported by Ahangari and Mashhadzadeh,[56] verifying H−H bond rupture and formation of new bonds with the cage atoms. For the encapsulated system $Y@B_{12}N_{12}{-}H_2$, structural deformation occurred, with displacement of the yttrium atom from the center to the outside of the cage. The thermodynamic properties ΔG_{ads} and ΔH_{ads} (298.15 K), adsorption energy (E_{ads}), and dipole moment (DM) are listed in Table 2. The $B_{12}N_{12}{-}H_2$ system showed positive ΔG_{ads} (+0.25 eV), characterizing nonspontaneous adsorption. After modification, all systems presented negative ΔG_{ads}, evidencing spontaneous adsorption. The ΔH_{ads} values were predominantly negative, indicating exothermic processes associated with intermolecular interactions, which reduce the energy and increase the stability of the system.

The adsorption energy (E_{ads}), obtained by eq 6, indicated physical adsorption for the $B_{12}N_{12}{-}H_2$ system (−0.04 eV). The nanocages modified with yttrium presented more negative values. However, the E_{ads} values of the $B_{12}N_{11}Y{-}H_2$, $Y@b_{66}{-}H_2$ and $Y@B_{12}N_{12}{-}H_2$ systems were higher (more negative) than −1.0 eV, thus limiting their application as sensors, as it makes the chemisorption process irreversible.[37,38] On the other hand, the decorated $Y@b_{64}{-}H_2$ system presented an adsorption energy value between − 0.3 eV < E_{ads} < −1.0 eV,[37,38] showing that the interaction between $Y@b_{64}$ and H_2 gas was a moderate chemisorption and suitable for application in H_2 detection. Regarding the H−H stretching frequency, a decrease was observed for systems without dissociation compared to the isolated H_2 molecule (ν_{H_2} = 4412.76 cm^{-1}), which also exhibit the lowest charges on the hydrogen atoms, as will be discussed later.

Table 2. Values of Gibbs Energy (ΔG_{ads}), Enthalpy of Adsorption (ΔH_{ads}), Adsorption Energy (E_{ads}), Dipole Moment (DM) and Stretching Frequencies H−H (ν_{H_2}) of Pure and Modified $B_{12}N_{12}$ after Adsorption with H_2 Gas

system	ΔG_{ads} (eV)	ΔH_{ads} (eV)	E_{ads} (eV)	DM (Debye)	ν_{H_2} (cm^{-1})
$B_{12}N_{12}{-}H_2$	+0.25	0.00	−0.04	0.16	4374.21
$YB_{11}N_{12}{-}H_2$	−0.16	−0.08	−0.15	10.53	4327.23
$B_{12}N_{11}Y{-}H_2$	−1.23	−1.61	−2.04	5.94	
$Y@b_{64}{-}H_2$	−0.40	−0.76	−0.96	0.83	
$Y@b_{66}{-}H_2$	−0.24	−1.85	−2.17	2.54	
$Y@B_{12}N_{12}{-}H_2$	−7.86	−8.03	−13.24	8.21	4371.54

3.3. Electronic Analysis

In Table 3, it is observed that the energies of the HOMO and LUMO orbitals of $B_{12}N_{12}$ underwent changes after the interaction with H_2, resulting in a direct variation of the energy gap (E_{gap}). The $B_{12}N_{12}$ gap presented a slight reduction, from 6.8 to 6.62 eV, corresponding to a variation of 2.67%, indicating low sensitivity and weak interaction with H_2. These results are corroborated by the low adsorption energy of the system (E_{ads} = −0.04 eV), characterizing a physisorption (E_{ads} > −0.3 eV) with van der Waals-type interaction.[57] The variation of the work function ($\Delta\Phi$), calculated by eq 8 and presented in Table 3, also indicates low sensitivity for the $B_{12}N_{12}{-}H_2$ system ($\Delta\Phi$ = 0.93%). In the yttrium-modified systems, the lowest value was

https://doi.org/10.1021/acsomega.5c11273
ACS Omega XXXX, XXX, XXX−XXX

Table 3. Values of HOMO-LUMO gap (E_{gap}), Sensitivity (ΔE_{gap}), Variation of the Work Function ($\Delta\Phi$), NPA Charge on the Y Atom (Q_{Metal}) and NPA Charge on the H Atoms (Q_{H_2}), of the Systems, Calculated for the Interaction of H_2 Gas with Pure and Modified $B_{12}N_{12}$

system	E_{gap} (eV)	ΔE_{gap} (%)	$\Delta\Phi$ (%)	Q_{Metal} (|e|)	Q_{H_2} (|e|)
$B_{12}N_{12}-H_2$	6.62	2.67	0.93	–	0.007
$YB_{11}N_{12}-H_2$	3.85	3.39	0.21	2.006	0.033
$B_{12}N_{11}Y-H_2$	2.60	2.61	2.09	1.606	−0.630
$Y@b_{64}-H_2$	2.57[a]	5.52[a]	36.62	1.782	−1.147
	5.12[b]	74.94[b]			
$Y@b_{66}-H_2$	1.46[a]	36.62[a]	26.88	1.350	−0.681
	4.82[b]	193.53[b]			
$Y@B_{12}N_{12}-H_2$	3.43[a]	65.47[a]	30.77	1.711	−0.002
	2.60[b]	11.78[b]			

[a]Spin up. [b]Spin down.

observed in $YB_{11}N_{12}-H_2$ ($\Delta\Phi$ = 0.21%), while the highest occurred in $Y@b_{64}-H_2$ ($\Delta\Phi$ = 36.62%), standing out as the most sensitive and promising system for work function-based sensor applications. These data confirm the high sensitivity between the $Y@b_{64}$ nanocage and the H_2 molecule.

The sensitivity of a system is evaluated by the variation of the band gap (ΔE_{gap}) before and after gas adsorption (eq 3), being influenced by the modification of the nanocage with yttrium. Pure $B_{12}N_{12}$ showed low sensitivity to H_2 (ΔE_{gap} = 2.67%; $\Delta\Phi$ = 0.93%; E_{ads} = −0.04 eV), characterizing physisorption. In the modified systems, the doped $B_{12}N_{11}Y-H_2$ was not very sensitive (ΔE_{gap} = 2.61%; $\Delta\Phi$ = 0.21%), while $Y@b_{66}-H_2$ (β-spin down), $Y@b_{64}-H_2$ (β-spin down) and $Y@B_{12}N_{12}-H_2$ (α-spin up) showed significant responses (ΔE_{gap} = 193.53%, 74.94% and 65.47%; $\Delta\Phi$ = 36.62% for $Y@b_{64}$). Considering E_{ads} and recovery time, $Y@b_{66}-H_2$ and $Y@B_{12}N_{12}-H_2$ (E_{ads} = −2.17 and −13.24 eV) are suitable for H_2 storage, as recently demonstrated by Sergio and Sousa for the $Y@b_{64}$ nanocage,[58] while $Y@b_{64}-H_2$ (E_{ads} = −0.96 eV) combines high sensitivity and moderate adsorption energy, being promising as a sensor. Furthermore, analysis of the NPA charges revealed that part of the charge transfers to the hydrogen atoms (with or without H_2 dissociation) originates from the nanocage. For example, in the $YB_{11}N_{12}-H_2$ system (undissociated H_2), the charge variation on the Y atom was −0.018 and that on H_2 was +0.033, whereas in the $Y@b_{64}-H_2$ system (dissociated H_2), the charge variation on the Y atom was +0.648 and that on H_2 was −1.147. This indicates a contribution from the nanocage to the overall charge-transfer process.

The results presented in Table S1 demonstrate that the magnetism induced by yttrium modification significantly affects H_2 activation, although it is not a necessary condition for molecular adsorption and dissociation. In the $Y@b_{64}$ and $Y@b_{66}$ decorated systems, the nanocage exhibits open-shell behavior prior to adsorption, with multiplicity 2, $\langle S^2\rangle \approx 0.75$, μ_{ef} in the range of 1.733−1.744 μ_B, and substantial spin populations on Y (0.939 and 0.840, respectively). After H_2 adsorption on the $Y@b_{64}$ nanocage, for example, a pronounced decrease in the metal spin population (0.939 → 0.282) is observed, accompanied by spin redistribution to the nanocage atoms and to the hydrogen atoms, which preferentially adsorb on yttrium (see Figure 3). This electronic reorganization is associated with the stronger adsorption energies observed for the decorated systems (−0.96 and −2.17 eV), reflecting the direct participation of partially occupied Y d orbitals in H_2 activation through σ(H−H) donation and back-donation into σ^*(H−H).[59]

On the other hand, H_2 dissociation does not depend exclusively on magnetism. The $B_{12}N_{11}Y$ nanocage, although

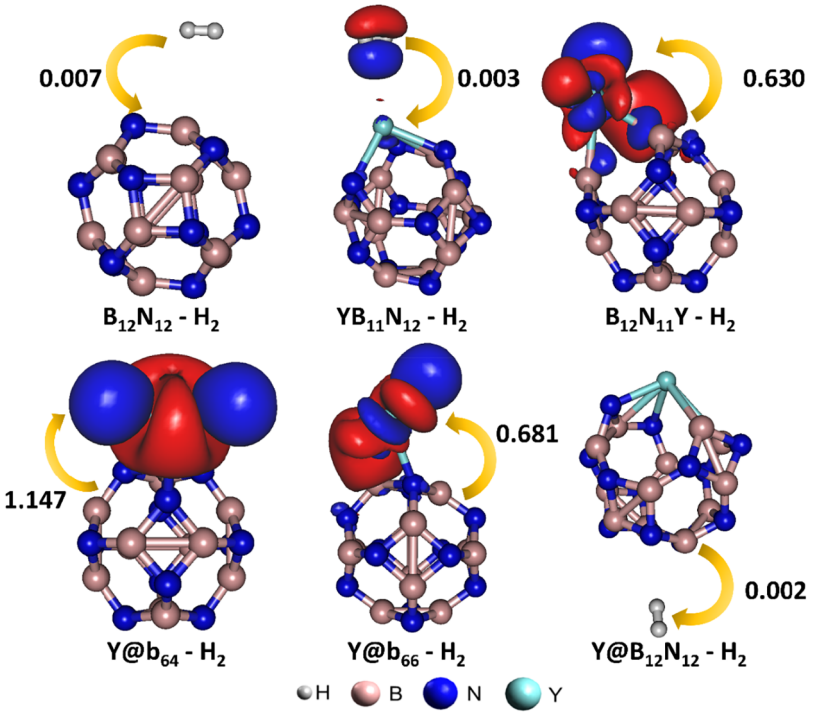

Figure 4. Charge density difference (CDD) of hydrogen gas adsorption on the surfaces of pure and Y-modified $B_{12}N_{12}$ nanocages with isosurface of 0.001 e·Å^{-3}. Red and blue colors represent charge accumulation and depletion, respectively. The arrows indicate the magnitude and direction of the electronic charge transfer.

https://doi.org/10.1021/acsomega.5c11273
ACS Omega XXXX, XXX, XXX−XXX

diamagnetic (μ_{ef} = 0, $\langle S^2 \rangle$ = 0), also promotes H−H bond cleavage, as evidenced by the significant negative NPA charges on hydrogen (−0.53 and − 0.09) and by the decrease in the Y electron population (37.7 → 37.4 e^-). In this case, the process is predominantly governed by charge transfer and electrostatic stabilization, independently of open-shell states. The encapsulated Y@$B_{12}N_{12}$ system exhibits an intermediate behavior: before adsorption, the spin population on Y is nearly negligible (0.008) with μ_{ef} = 2.645 μ_B, but upon interaction with H_2, local magnetism is induced, increasing the spin on the metal to 0.17 and on the hydrogen atoms to 0.98, consistent with the absence of H_2 dissociation on the Y@$B_{12}N_{12}$ surface. Overall, these results indicate that magnetism plays a central role in the adsorption process, either enhancing the H_2-nanocage interaction or being induced by adsorption itself, depending on the doping topology and the initial electronic distribution.[60]

To elucidate the electronic interactions associated with H_2 adsorption on the surfaces of the pristine and Y-modified $B_{12}N_{12}$ nanocages, charge density difference (CDD) calculations were performed for the nanocage-H_2 systems and the corresponding results are shown in Figure 4. It was observed that the interactions between the $B_{12}N_{11}Y$, Y@b_{64}, and Y@b_{66} nanocages and the H_2 molecule were more effective, as confirmed by the substantial NPA charge transfers occurring upon adsorption. In these cases, H_2 dissociation on the nanocage surfaces was identified; however, the most pronounced charge transfer was found in the Y@b_{64}−H_2 system, primarily because the two hydrogen atoms remained bonded to the yttrium atom, in contrast to what was observed in the $B_{12}N_{11}Y$−H_2 and Y@b_{66}−H_2 systems (see Figure 3). The FMO analysis in Figure 5 highlights the electronic distribution and supports the interpretation of gas-nanocage interactions for Y@b_{64} nanocages with H_2 gas.

The HOMO presents electron density uniformly distributed over the B and N cage, while the LUMO is slightly concentrated in the peripheral regions of the $B_{12}N_{12}$ nanocage. This distribution indicates weak electronic polarization and limited interaction with H_2, consistent with the observed low adsorption

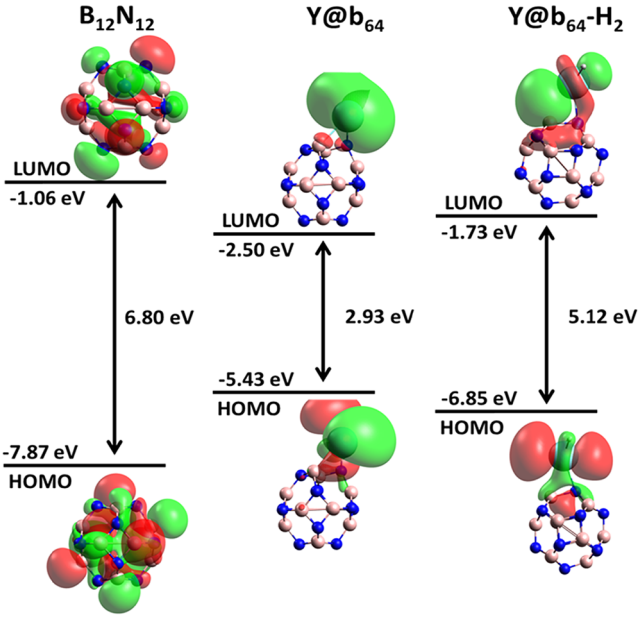

Figure 5. HOMO and LUMO of pure $B_{12}N_{12}$ and Y@b_{64} nanocages before and after H_2 adsorption.

energy (E_{ads} = −0.04 eV), small band gap variation (ΔE_{gap} = 2.67%), and low work function variation ($\Delta\Phi$ = 0.93%). In the Y@b_{64} nanocage, the HOMO shows accumulation of electron density near the yttrium atom, suggesting that yttrium acts as an active center for interaction with gases. The LUMO is concentrated in regions close to yttrium and the nanocage, favoring partial charge transfer with H_2. This explains the higher observed sensitivity (ΔE_{gap} = 74.94%) and the moderate adsorption energy (E_{ads} = −0.96 eV). After H_2 adsorption, the HOMO and LUMO orbitals overlap between H_2 and the doped nanocage, indicating a more significant chemical interaction than in the pure system. The electronic redistribution demonstrates the system's responsiveness to the presence of H_2, corroborating the high work function variation ($\Delta\Phi$ = 36.62%) and the adequate adsorption energy for sensing.

The DOS analysis of both pristine and Y-modified $B_{12}N_{12}$ nanocages after hydrogen gas adsorption is presented in Figure S1 in Supporting Information. The DOS plots reveal that upon interaction with H_2, the $B_{12}N_{12}$ nanocage experiences slight HOMO destabilization and LUMO stabilization, leading to a reduction in its energy gap from 6.80 to 6.62 eV. Additionally, all yttrium-modified nanocages exhibited an increase in E_{gap} values after H_2 adsorption compared to the values of the pure nanocages. These findings further support the conclusion that the modified systems are more reactive than the pristine $B_{12}N_{12}$ nanocage, as evidenced by the previously discussed parameters.

3.4. Quantum Descriptors and Stability

The values of chemical potential (μ), chemical hardness (η), softness (S), ionization potential (IP), electron affinity (eA), and electrophilicity (ω) for the isolated systems were calculated by applying eqs 10−15 and are listed in Table 4, as well as for the

Table 4. Quantum Descriptors: Chemical Hardness (η), Softness (S), Ionization Potential (IP), Electron Affinity (eA), Chemical Potential (μ), Electrophilicity (ω)

system	IP (eV)	eA (eV)	η (eV)	μ (eV)	S (eV^{-1})	ω (eV)
$B_{12}N_{12}$	7.84	1.07	3.38	−4.46	0.15	2.94
$B_{12}N_{12}$−H_2	7.82	1.19	3.31	−4.50	0.15	3.06
$YB_{11}N_{12}$	6.73	2.67	2.03	−4.70	0.25	5.44
$YB_{11}N_{12}$−H_2	6.63	2.78	1.92	−4.71	0.26	5.76
$B_{12}N_{11}Y$	5.10	2.56	1.27	−3.83	0.39	5.79
$B_{12}N_{11}Y$−H_2	5.05	2.45	1.30	−3.75	0.38	5.42
Y@b_{64}	4.35	1.92	1.22	−3.14	0.41	4.04
Y@b_{64}−H_2	6.85	1.73	2.56	−4.29	0.20	3.60
Y@b_{66}	4.40	1.97	1.22	−3.18	0.41	4.16
Y@b_{66}−H_2	3.45	1.99	0.73	−2.72	0.68	5.07
Y@$B_{12}N_{12}$	4.41	2.40	1.01	−3.41	0.50	5.77
Y@$B_{12}N_{12}$−H_2	6.18	2.75	1.71	−4.46	0.29	5.81

modified nanocages after gas adsorption. Initially, it is highlighted that the value of the chemical potential is negative in all conditions, implying the stability of the structures and the spontaneity of all processes.[61] The results show that the pure $B_{12}N_{12}$ has the highest hardness (η = 3.38 eV) and the lowest softness (S = 0.15 eV^{-1}) and electrophilicity (ω = 2.94 eV). These results agree with values published in previous studies.[62−64] It also shows a higher ionization potential compared to the doped structures, whereas the electron affinity increases upon modification, revealing an enhanced electron-accepting capability. Chemical hardness (η) is associated with a system's resistance to changes in its electronic distribution;[65]

https://doi.org/10.1021/acsomega.5c11273
ACS Omega XXXX, XXX, XXX−XXX

therefore, larger HOMO−LUMO gaps correspond to more rigid and less reactive systems. Conversely, softness (S) characterizes the tendency to accept electronic charge and is inversely related to hardness.[66] Consequently, systems with smaller HOMO−LUMO gaps become more polarizable and reactive, as observed for Y@$B_{12}N_{12}$, whose behavior is consistent with its higher adsorption energy in the Y@$B_{12}N_{12}$−H_2 complex. Among the investigated systems, $B_{12}N_{12}$−H_2 showed the lowest softness (S = 0.15 eV^{-1}), whereas Y@b_{66}−H_2 exhibited the highest value (S = 0.68 eV^{-1}). In terms of hardness, Y@b_{66}−H_2 displayed the lowest value (η = 0.73 eV), while $B_{12}N_{12}$−H_2 retained the highest hardness (η = 3.31 eV).[67] The Y@b_{64}−H_2 system presented intermediate values of chemical potential (μ = −4.29 eV), softness (S = 0.20 eV^{-1}), and electrophilicity (ω = 3.60 eV).

3.5. Electrostatic Potential Analysis

In Figure 6 presents the Molecular Electrostatic Potential (MEP) for the optimized Y@b_{64} and Y@b_{64}−H_2 structures.

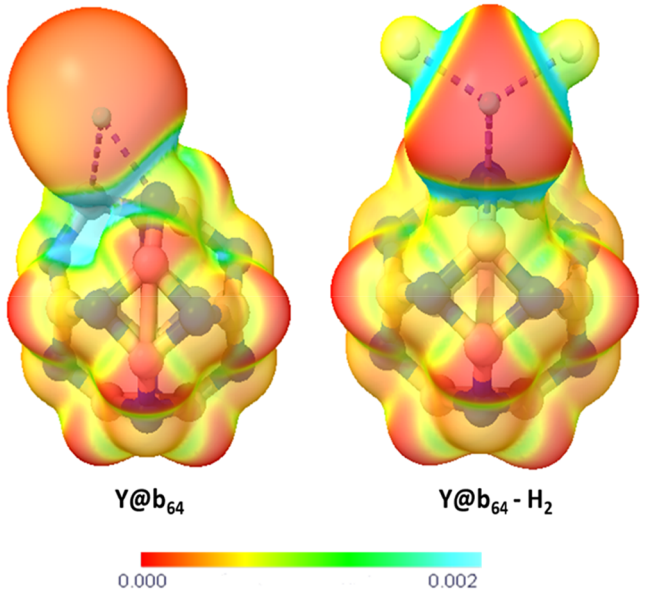

Figure 6. Molecular electrostatic potential (MEP) map of the Y@b_{64} nanocage and the Y@b_{64}−H_2 adsorption system.

This analysis demonstrates the variations in the electronic density of the nanocage after modification with Y and adsorption of hydrogen gas, revealing charge distributions as well as the electrophilic and nucleophilic regions of the molecules.[68]

The MEP is directly associated with physicochemical properties, such as partial charges, dipole moment, and chemical reactivity. In the analyzed systems, the MEP maps show distinct regions: red and yellow indicate negative charges, corresponding to nucleophilic sites; blue represents positive charges, characterizing electrophilic sites; and light green corresponds to neutral areas.[69,70] According to Janjua,[71] in the pristine $B_{12}N_{12}$ nanocage, the boron atoms exhibit a positive electrostatic potential (blue regions), whereas the nitrogen atoms display a negative potential (yellow regions). The $B_{12}N_{12}$ structure is highly symmetrical and presents a homogeneous charge distribution, which explains its zero dipole moment. Moreover, it was found that H_2 adsorption on $B_{12}N_{12}$ does not induce significant charge redistribution, indicating a weak interaction between the gas and the nanocage.

In this study, the Y@b_{64} decorated structure shows a clear modification in the charge distribution pattern, with the region associated with the yttrium atom exhibiting a nucleophilic character (red regions). After H_2 adsorption, electrophilic regions emerge along the Y−H bonds, as well as intermediate neutral areas, revealing a stronger interaction between the gas and the modified surface, compared to the interaction of $B_{12}N_{12}$ with H_2.

3.6. Thermodynamic Stability Study

Molecular dynamics (MD) analysis was performed in the 0−1000 ps time range, a methodology similar to that employed by De Sousa Sousa et al.[72] It is noteworthy that this time interval is sufficient to observe possible configurational changes. The stability of the Y@b_{64} nanocage was evaluated before and after the interaction with H_2, as shown in Figure 7. Previous results by Kundu and Chakraborty[23] demonstrated that yttrium-doped triazine structures maintain their integrity at high temperatures (420 K), allowing the stable adsorption of up to seven H_2 molecules per Y atom at 300 K. Similarly, the results obtained for Y@b_{64}−H_2 show that the gas remains adsorbed on the cage surface, presenting only small energetic variations, attributed to geometric adjustments and H_2 rotations. This stability throughout the simulation confirms the potential of the Y@b_{64} nanocage as a gas sensor, corroborating the chemical interaction data (E_{ads} = −0.96 eV) and electronic sensitivity (ΔE_{gap} = 74.94%).

3.7. Optical Analysis

The absence of negative frequencies in the spectra confirms the stability of the analyzed geometries (for a more detailed analysis, all frequency values before and after interaction with the H_2 molecule are presented in Table S2, and the corresponding IR

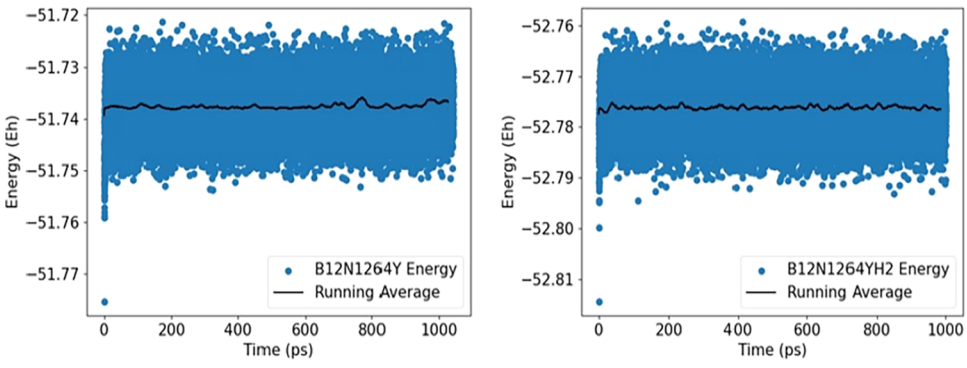

Figure 7. Quantum molecular dynamics trajectory for the Y@b_{64} nanocage before and after interaction with H_2 gas.

https://doi.org/10.1021/acsomega.5c11273
ACS Omega XXXX, XXX, XXX−XXX

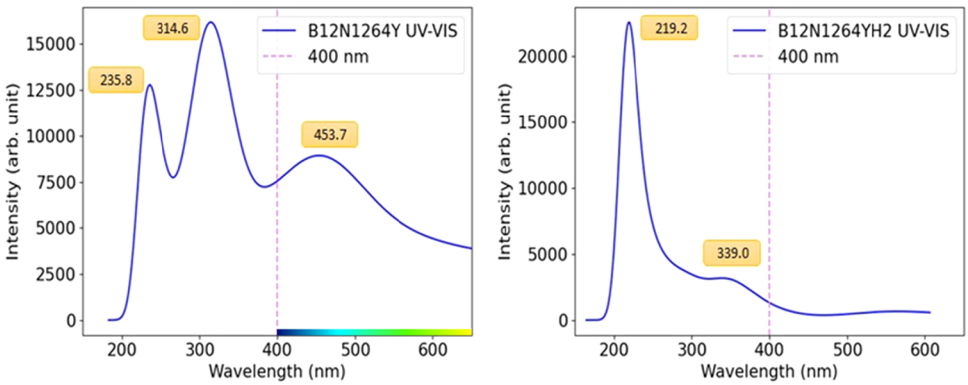

Figure 8. UV−vis spectrum of the Y@b_{64} nanocage before and after H_2 gas adsorption.

spectra before and after H_2 adsorption are shown in Figures S2 and S3). The vibrational modes located at approximately 706 and 1632 cm^{-1} correspond to the B−N stretching and B−N bending modes, respectively.[73] After the adsorption of the H_2 molecule on the surface of the Y@b_{64} nanocage, the appearance of a peak at 1619 cm^{-1} is observed, which is characteristic of the Y−H interaction.[74]

UV−vis spectroscopy is widely used to monitor adsorption processes. Nair et al.,[75] for example, applied this technique to monitor the adsorption of 5FU on PLGA. In Figure 8 shows that the Y@b_{64} nanocage exhibits three absorption peaks. The first occurs at 235.8 nm, associated with an excitation energy of E = 5.2, with a predominant electronic contribution from the H(α) → L(α) transition (49%). The second peak is observed at 314.6 nm, corresponding to E = 3.8, resulting from the HOMO → LUMO transitions [H(α) → L(α) (27%) and H−1(α) → L+1(α) (25%)]. The third peak appears at 453.7 nm, associated with E = 2.5, with a greater contribution from the H(α) → L(α) transition (72%). After adsorption of the H_2 molecule, the Y@b_{64}−H_2 system presented a maximum absorbance peak at λ_{max} = 219.2 nm, corresponding to an excitation energy of E = 5.6, with contributions from the transitions [H(β) → L(β) (26%) and H−1(β) → L+1(β) (20%)]. Furthermore, a peak was identified at λ_{min} = 339.0 nm, associated with E = 3.5, with electronic transition [H(α) → L(α) (83%)].[76] Wavelengths (λ_{max}), oscillator intensities (f), energies (E), and main electronic transitions associated with the absorption peaks of the Y@b_{64} and Y@b_{64}-H_2 systems are presented in Table S3. The spectral shift thus provides a promising experimental signature for in situ validation of gas adsorption via UV−vis.

The changes in the UV−vis spectrum of the Y@b_{64}−H_2 system occur due to the absorption of the H_2 molecule by the Y atom. The results indicate that the yttrium-decorated nanocage Y@b_{64} exhibits optical sensitivity to H_2 gas, suggesting that this material possesses characteristics suitable for application in optical hydrogen gas detection.

3.8. Study of Adsorption of Interfering Gases

The selectivity of the Y@b_{64} nanocage for H_2 was evaluated relative to some interfering gases commonly used in previous experimental studies reported in the literature (CH_4, CO, H_2S, and N_2)[24,25,77,78] (see Figure 9). The adsorption distances showed that H_2 interacts more strongly (d = 1.98 Å) than the interfering gases, which presented larger distances (2.39 to 3.56 Å) and weak interactions. The NPA charge analysis of the interfering gases showed that the charge variation on the Y atom was 1.782, whereas for the H_2 molecule it was −1.147, indicating a significantly greater charge transfer from the Y@b_{64} nanocage

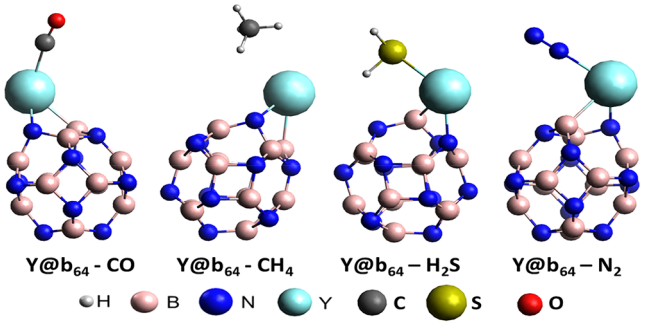

Figure 9. Optimized structures of the adsorption of Y@b_{64} nanocage with interfering gases CO, CH_4, H_2S, and N_2.

to H_2 compared with the gases CO, CH_4, H_2S, and N_2. H_2 adsorption (E_{ads} = −0.96 eV) characterizes chemisorption, with an adequate recovery time (τ = 166.8 s), while the interferents present very short recovery times. These results confirm the high selectivity and efficiency of Y@b_{64} in the detection of hydrogen gas. However, as pointed out by Kaewmaraya et al.,[38] we need to treat the calculated binding energy with caution because this value is based on the single molecule adsorption which does not take into, for example, the factor of gas concentration feeding to the sensor.

The ΔE_{gap} results show that the Y@b_{64} nanocage presents greater sensitivity to hydrogen gas compared to the other gases evaluated (ΔE_{gap} = 74.94%), indicating that the system preferentially detects H_2 (data presented in Table 5). The variation in the free energy of adsorption (ΔG_{ads}) confirms that the adsorption processes are spontaneous for all gases studied, except for methane (ΔG_{ads} = +0.32 eV), characterized as nonspontaneous. Selectivity was analyzed by calculating the sensor response (S) and the selectivity coefficient (κ), according to eqs 17 and 18, parameters that express the efficiency of the system in the selective detection of H_2 compared to the tested atmospheric gases. Greater selectivity was observed for the H_2/CH_4 pair, reinforcing the lower detection of methane and confirming the high sensitivity of Y@b_{64} to hydrogen gas.

Table 6 shows the performance of different nanomaterials in H_2 detection reported in the literature,[11,79−88] whose adsorption energies range from −0.072 to −1.830 eV. Values in the range −0.3 eV < E_{ads} < −1.0 eV are considered ideal for sensor applications.[37,38,57] Pure $B_{12}N_{12}$ presented E_{ads} = −0.072 eV, characterizing physisorption, a behavior similar to other nanomaterials, such as AlP-doped graphene (E_{ads} = −0.218 eV), NiN_4S-doped SWCNT (E_{ads} = −0.082 eV), and $C_{16}Mg_8O_8$ nanocage (E_{ads} = −0.170/−0.114 eV). It is noteworthy that the

https://doi.org/10.1021/acsomega.5c11273
ACS Omega XXXX, XXX, XXX−XXX

Table 5. Values of Gap HOMO-LUMO (E_{gap}), Cage/Gas Distance (d), NPA Charge on the Y Atom (Q_{Metal}) and NPA Charges on the Atoms of Interfering Gases (Q_{gas}), Adsorption Energy (E_{ads}), Electronic Sensitivity (ΔE_{gap}), Free Energy of Adsorption (ΔG_{ads}), Recovery Time (τ), the Sensitivity (S) and Selectivity Coefficient (κ) Calculated for the Interaction of CO, CH_4, H_2S, and N_2 Gases with the $Y@b_{64}$ Cage

system	E_{gap} (eV)	d (Å)	Q_{Metal} (|e|)	Q_{gas} (|e|)	E_{ads} (eV)	ΔE_{gap} (%)	ΔG_{ads} (eV)	τ	S	κ
$Y@b_{64}$–H_2	5.12	1.98	1.782	−1.147	−0.96	74.94	−0.40	166.80 s	3.19×10^{18}	
$Y@b_{64}$–CO	1.77	2.39	1.413	0.002	−0.62	27.12	−0.03	299.87 μs	6.33×10^{9}	5.04×10^{8}
$Y@b_{64}$–CH_4	3.01	3.56	1.170	−0.295	−0.06	2.76	+0.32	103.25 fs	3.74	8.53×10^{17}
$Y@b_{64}$–H_2S	2.32	2.83	1.110	0.052	−0.65	4.65	−0.04	963.55 μs	1.43×10^{5}	2.23×10^{13}
$Y@b_{64}$–N_2	1.75	2.39	1.258	−0.177	−0.33	28.00	−0.07	3.77 ns	9.33×10^{9}	3.42×10^{8}

Table 6. Comparison of Sensing Materials for the Detection of Hydrogen Gas (H_2)

sensor	functional	E_{ads} (eV)	ΔE_{gap} (%)	τ (s)	other gases	refs
$B_{12}N_{12}$ nanocage	B3LYP-D4	−0.072	5×10^{-3}[a]		CO_2	Choir et al.[11]
$C_{16}Mg_8O_8$ nanocage	M06-D3	−0.170	0.54[a]		N_2	Ghamsari et al.[79]
	B97D	−0.114	3.45[a]			
rGO-ZnO–Ag-Pd film	GGA-PBE	−0.720	59.00[c]	14.00		Pal et al.[80]
W-doped graphene	GGA-PBE-D2	−1.035	24.85[b]	2.44×10^{5}	NH_3, CH_4, CO, SO_2 and H_2S	Yang et al.[81]
AlP-decorated graphene	M06–2X	−0.218	4.68[b]	4.65×10^{-9}		Zakeri et al.[82]
Pt-doped g-C_3N_4	GGA-PBE	−1.830	26.19[a]		CH_4 and CO_2	Luo et al.[83]
Pt-ZnONT	B3LYP-D3	−1.360	4.19[a]	1.35×10^{-9}[d]		Li and Asad[84]
Pt-decorated WS_2	GGA-PBE-D	−1.300	27.00[a]	1.85[e]	CO, H_2S, NH_3, and CH_4	Li et al.[85]
Pt-doped $MoTe_2$	GGA-PBE-D	−1.791	12.41	1.32×10^{6}[f]	CO, C_2H_4, and C_2H_2	Jiang et al.[86]
NiN_4S-doped SWCNT	ωB97XD	−0.082	50.94[b]	2.20×10^{-11}		Imeni et al.[87]
$Al_{12}C_{12}$ nanocage	B3LYP	H_2–Al = −0.550	0.21[c]	1.97×10^{-3}	CH_4, CO, NO, and NH_3	Huang et al.[88]
		H_2–C = −0.560	0.21[c]	2.90×10^{-3}		
$Y@b_{64}$	B3LYP-D3	−0.960	74.94	166.80	CH_4, CO, H_2S, and N_2	this work

[a]Value calculated from E_{gap} data. [b]Value found in the article. [c]Value calculated by the equation $S = [(R - R_0)/R_0] \times 100\%$. [d]Value calculated at 598 K. [e]Value calculated at 538 K. [f]Value calculated at 498 K.

rGO-ZnO–Ag-Pd film and $Al_{12}C_{12}$ nanocage systems, despite presenting adequate adsorption energies and recovery times, as well as the $Y@b_{64}$–H_2 system (E_{ads} = −0.96 eV and τ = 166.8 s), proposed in this work. The $Y@b_{64}$ nanocage, in comparison to the systems presented in Table 6, presented the highest electronic sensitivity to H_2 (ΔE_{gap} = 74.94%), in addition to being selective to CH_4, CO, H_2S and N_2 gases, positioning the $Y@b_{64}$ nanocage as a promising material for application in selective H_2 gas sensors.

The comparison among different theoretical studies of H_2 sensors highlights the central role of computational modeling in identifying materials with superior performance in terms of sensitivity, selectivity, and stability. The detailed evaluation of electronic, structural, and adsorption properties not only guides the rational selection of promising candidates but also reduces experimental costs and directs the development of more efficient devices. These advances hold potential for application in leak-monitoring systems, safety devices for hydrogen production, and technologies associated with fuel cells. Thus, theoretical results not only deepen the understanding of detection mechanisms but also strengthen the integration between computational research and the implementation of technological solutions, driving the transition toward the growing hydrogen economy.

4. CONCLUSIONS

In this study, density functional theory (DFT) and time-dependent DFT (TD-DFT) calculations revealed that yttrium modification of $B_{12}N_{12}$ nanocages significantly enhances H_2 adsorption performance. Geometric, electronic, energetic and optical properties were analyzed, and the results presented that while the pristine $B_{12}N_{12}$ nanocage exhibited weak physisorption (E_{ads} = −0.04 eV; ΔG_{ads} = +0.25 eV), all Y-modified configurations displayed spontaneous adsorption ($\Delta G_{ads} < 0$) with markedly increased interaction energies. Among the studied systems, the $Y@b_{64}$–H_2 configuration exhibited chemisorption (E_{ads} = −0.96 eV) with adequate recovery time (τ = 166.8 s), substantial electronic sensitivity (ΔE_{gap} = 74.94%), structural stability under molecular dynamics simulations, and a detectable optical response in the UV–Vis region. Furthermore, it demonstrated superior selectivity against common interfering gases (CH_4, CO, H_2S, and N_2), highlighting its potential as a dual-mode electronic and optical H_2 sensor. These results position $Y@b_{64}$ as a highly promising candidate for hydrogen monitoring and industrial safety applications. Experimental validation will be essential to confirm these theoretical predictions under practical conditions, particularly in industrial safety and hydrogen monitoring environments. Future directions include investigating the integration of this material into real sensing platforms, as well as assessing its performance in miniaturized devices operating under variable environmental conditions, targeting applications in intelligent detection networks and in the emerging infrastructure of the hydrogen economy.

■ ASSOCIATED CONTENT

Supporting Information

The Supporting Information is available free of charge at https://pubs.acs.org/doi/10.1021/acsomega.5c11273.

DOS of hydrogen gas adsorption on pure $B_{12}N_{12}$, $YB_{11}N_{12}$, $B_{12}N_{11}Y$, $Y@b_{64}$, $Y@b_{66}$ and $Y@B_{12}N_{12}$ nanocages (Figure S1); IR spectra of the of the $B_{12}N_{12}$ nanocage and the yttrium metal-modified nanocages:

https://doi.org/10.1021/acsomega.5c11273
ACS Omega XXXX, XXX, XXX−XXX

doped ($YB_{11}N_{12}$ and $B_{12}N_{11}Y$), decorated ($Y@b_{64}$ and $Y@b_{66}$), and encapsulated ($Y@B_{12}N_{12}$) (Figure S2); IR spectra of the hydrogen gas (H_2) adsorption on the surfaces of pure and Y-modified $B_{12}N_{12}$ nanocages (Figure S3); Multiplicity, sum spin population, Mulliken Spin Population, Electron Population, S^2, deviation, effective magnetic moment (μ_{ef}), and magnetism for all systems studies (Table S1); Vibrational frequencies (cm^{-1}) for all systems studies (Table S2); Wavelengths (λ_{max}), oscillator intensities (f), energies (E), and main electronic transitions associated with the absorption peaks of the $Y@b_{64}$ and $Y@b_{64}$-H_2 systems (Table S3) (PDF)

AUTHOR INFORMATION

Corresponding Author

Adilson Luís Pereira Silva − *Universidade Estadual do Maranhão, 65055-310 São Luís, MA, Brazil;* orcid.org/0000-0002-8824-9980; Email: adlpsilva@gmail.com

Authors

Wellington da Conceição Lobato do Nascimento − *Universidade Federal do Maranhão, 65080-805 São Luís, MA, Brazil*

Natanael de Sousa Sousa − *Universidade Federal do Maranhão, 65080-805 São Luís, MA, Brazil;* orcid.org/0009-0002-5913-4735

Adeilton Pereira Maciel − *Universidade Federal do Rio Grande do Norte, 59078-970 Natal, RN, Brazil*

Complete contact information is available at: https://pubs.acs.org/10.1021/acsomega.5c11273

Funding

The Article Processing Charge for the publication of this research was funded by the Coordenacao de Aperfeicoamento de Pessoal de Nivel Superior (CAPES), Brazil (ROR identifier: 00x0ma614).

Notes

The authors declare no competing financial interest.

ACKNOWLEDGMENTS

This work was supported by the following Brazilian research agencies: Conselho Nacional de Desenvolvimento Científico e Tecnológico (CNPq), Conselho Nacional de Aperfeiçoamento do Ensino Superior (CAPES) and the Fundação de Amparo à Pesquisa e ao Desenvolvimento Científico e Tecnológico do Maranhão (FAPEMA). The first author receives a grant from FAPEMA (BD-05177/23).

REFERENCES

(1) Zhu, M.; Zhang, H.; Zhang, S.; Yao, H.; Shi, X.; Xu, S. Chemoresistive gas sensors based on noble-metal-decorated metal oxide semiconductors for H_2 detection. *Materials* **2025**, *18*, No. 451.

(2) Benitto, J. J.; Akash, K.; Vijaya, J. J.; Humayun, M.; Bououdina, M. State-of-the-Art Hydrogen Gas Sensors: From Fundamentals to Applications. *J. Electron. Mater.* **2025**, *54*, 879−909.

(3) de Sousa Sousa, N.; Silva, A. L. P.; de Jesus Gomes Varela Júnior, J.; Rodrigues, N. M. Theoretical Study of SO_2 Selective Detection from the Cr-Modified $B_{12}N12$. *ACS Omega* **2025**, *10*, 31789−31800.

(4) Wang, X.; Zhu, Y.; Gao, W. Design of hydrogen sensor relying on Pd-MWCNT/WO_3 sensing materials for selective and rapid hydrogen detection. *Sens. Actuators, B* **2025**, *422*, No. 136648.

(5) Liu, Y.; Zhi, Z.; Liu, S.; Qian, J.; Huang, K.; Hua, Z. Room Temperature Ionic Liquid-Gated Carbon Nanotube FETs for Stable Hydrogen Sensing at Elevated Temperatures. *ACS Omega* **2025**, *10*, 27462−27472.

(6) Khan, J. A.; Ghosh, S.; Sanyal, D. H_2 adsorption over GeO_2 monolayer: a theoretical study. *J. Mater. Sci.: Mater. Eng.* **2025**, *20*, No. 119.

(7) Li, Q.; Wang, L.; Xiao, A.; Zhu, L.; Yang, Z. Hydrogen sensing towards palladium-based nanocomposites: A review. *Int. J. Hydrogen Energy* **2025**, *136*, 1282−1305.

(8) Nair, R. G. S.; Nair, A. K. N.; Sun, S. Adsorption of Gases on Fullerene-like $X_{12}Y_{12}$ (X = Be, Mg, Ca, B, Al, Ga, C; Y = C, Si, N, P, O) Nanocages. *Energy Fuels* **2023**, *37*, 14053−14063.

(9) Aasi, A.; Javahersaz, R.; Aghaei, S. M.; Panchapakesan, B. Novel green phosphorene as a superior gas sensor for dissolved gas analysis in oil transformers: using DFT method. *Mol. Simul.* **2022**, *48*, 541−550.

(10) Kalateh, K.; Cordshooli, G. A.; Kheirollahpoor, S. Hydrogen adsorption, structural, electronic, and spectroscopic properties of C_{32}, $B_{16}N_{16}$, and B_8C_{24} by DFT calculations. *Fullerenes, Nanotubes Carbon Nanostruct.* **2017**, *25*, 459−465.

(11) Choir, A. A.; Amelia, S. R.; Martoprawiro, M. A.; Kusumawati, Y.; Ivansyah, A. L. Insight into the adsorption properties of CO_2 and H_2 gas on the $B_{12}Y_{12}$ (Y - N, P, As, Sb) nanocages from a host-guest interaction perspective. *Int. J. Hydrogen Energy* **2024**, *53*, 780−791.

(12) Nair, R. G. S.; Nair, A. K. N.; Sun, S. Adsorption of gases on $B_{12}N_{12}$ and $Al_{12}N_{12}$ nanocages. *New J. Chem.* **2024**, *48*, 8093−8105.

(13) Silva, A. L. P.; Sousa, N. S.; de Jesus Gomes Varela Júnior, J. Theoretical studies with $B_{12}N_{12}$ as a toxic gas sensor: a review. *J. Nanopart. Res.* **2023**, *25*, No. 22.

(14) de Sousa Sousa, N.; Silva, A. L. P.; Silva, A. C. A.; de Jesus Gomes Varela Júnior, J. Cu-modified $B_{12}N_{12}$ nanocage as a chemical sensor for nitrogen monoxide gas: a density functional theory study. *J. Nanopart. Res.* **2023**, *25*, No. 248.

(15) Silva, A. L. P.; de Jesus Gomes Varela Júnior, J. $MB_{11}N_{12}$ (M = Fe−Zn) Nanocages for Cyanogen Chloride Detection: A DFT Study. *J. Inorg. Organomet. Polym. Mater.* **2024**, *34*, 302−312.

(16) Qadir, K. W.; Mohammadi, M. D.; Ridha, N. J.; Abdullah, H. Y. Determining the binding mechanism of $B_{12}N_{12}$(Zn) with CH_4, CO, CO_2, H_2O, N_2, NH_3, NO, NO_2, O_2, and SO_2 gases. *Microporous Mesoporous Mater.* **2024**, *379*, No. 113289.

(17) Rakrai, W.; Tabtimsai, C.; Kaewtong, C.; Chuekachang, S.; Keawwangchai, S.; Keawwangchai, T.; Wanno, B. Hydrogen storage and sensing ability of group 8B transition metal-doped $B_{12}N_{12}$ nanocages: a DFT investigation. *Struct. Chem.* **2024**, *35*, 437−453.

(18) Oku, T.; Nishiwaki, A.; Narita, I. Formation and atomic structure of $B_{12}N_{12}$ nanocage clusters studied by mass spectrometry and cluster calculation. *Sci. Technol. Adv. Mater.* **2004**, *5*, 635−645.

(19) Oku, T.; Kuno, M.; Kitahara, H.; Narita, I. Formation, atomic structures and properties of boron nitride and carbon nanocage fullerene materials. *Int. J. Inorg. Mater.* **2001**, *3*, 597−612.

(20) Oku, T.; Narita, I.; Nishiwaki, A.; Koi, N. Atomic structures, electronic states and hydrogen storage of boron nitride nanocage clusters, nanotubes nanohorns. *Defect Diffus. Forum* **2004**, *226*, 113−140.

(21) Oku, T.; Narita, I.; Nishiwaki, A. Formation and structures of $B_{36}N_{36}$ and $Y@B_{36}N_{36}$ clusters studied by high-resolution electron microscopy and mass spectrometry. *J. Phys. Chem. Solids* **2004**, *65*, 369−372.

(22) Wang, T.; Tian, Z. Yttrium-decorated $C_{48}B_{12}$ as hydrogen storage media: A DFT study. *Int. J. Hydrogen Energy* **2020**, *45*, 24895−24901.

(23) Kundu, A.; Chakraborty, B. Yttrium doped covalent triazine frameworks as promising reversible hydrogen storage material: DFT investigations. *Int. J. Hydrogen Energy* **2022**, *47*, 30567−30579.

(24) Srivastava, S.; Pandy, N. K.; Verma, V.; Singh, P.; Verma, A.; Yadav, N.; Pandey, P. K.; Sarkar, J. Development of Yttrium-Cerium oxide gas sensor for low ppm Hydrogen detection. *ASEC 2023* **2023**, *56*, No. 120.

https://doi.org/10.1021/acsomega.5c11273
ACS Omega XXXX, XXX, XXX−XXX

(25) Ferlazzo, A.; Espro, C.; Iannazzo, D.; Moulaee, K.; Neri, G. A novel yttria-doped ZrO_2 based conductometric sensor for hydrogen leak monitoring. *Int. J. Hydrogen Energy* **2022**, *47*, 9819−9828.
(26) Neese, F. Software update: The ORCA program system−Version 5.0. *WIREs Comput. Mol. Sci.* **2022**, *12*, No. e1606.
(27) Grimme, S. Semiempirical GGA-type density functional constructed with a long-range dispersion correction. *J. Comput. Chem.* **2006**, *27*, 1787−1799.
(28) Grimme, S. Density functional theory with London dispersion corrections. *WIREs Comput. Mol. Sci.* **2011**, *1*, 211−228.
(29) Onsori, S.; Liyaghati-Delshad, M. The effects of different Minnesota functionals on the sensitivity of boron nitride nanocluster to nitrogen dioxide. *Chem. Phys. Lett.* **2017**, *680*, 22−27.
(30) Farrokhpour, H.; Jouypazadeh, H.; Sohroforouzani, S. V. Interaction of different types of nanocages ($Al_{12}N_{12}$, $Al_{12}P_{12}$, $B_{12}N_{12}$, $Be_{12}O_{12}$, $Mg_{12}O_{12}$, $Si_{12}C_{12}$ and C_{24}) with HCN and ClCN: DFT, TD-DFT, QTAIM, and NBO calculations. *Mol. Phys.* **2020**, *118*, No. e1626506.
(31) Silva, A. L. P.; de Jesus Gomes Varela Júnior, J. Density Functional Theory Study of Cu-Modified $B_{12}N_{12}$ Nanocage as a Chemical Sensor for Carbon Monoxide Gas. *Inorg. Chem.* **2023**, *62*, 1926−1934.
(32) Hossain, M. R.; Hasan, M. M.; Nishat, M.; Noor-E-Ashrafi; Ahmed, F.; Ferdous, T.; Hossain, M. A. DFT and QTAIM investigations of the adsorption of chlormethine anticancer drug on the exterior surface of pristine and transition metal functionalized boron nitride fullerene. *J. Mol. Liq.* **2021**, *323*, No. 114627.
(33) de Sousa Sousa, N.; Silva, A. L. P. Novel structures of boron and nitrogen-based nanocapsules: DFT insights. *Comput. Theor. Chem.* **2025**, *1252*, No. 115402.
(34) Redondo, A.; Zeiri, Y.; Lowand, J. J.; Goddard, W. A. Application of transition state theory to desorption from solid surfaces: Ammonia on Ni (111). *J. Chem. Phys.* **1983**, *79*, 6410−6415.
(35) Zahedi, E.; Seif, A.; Ahmadi, T. S. Structural and Electronic Properties of Ammonia Adsorption on the $C_{30}B_{15}N_{15}$ Heterofullerene: A Density Functional Theory Study. *J. Comput. Theor. Nanosci.* **2011**, *8*, 2159−5165.
(36) Koettgen, J.; Zacherle, T.; Grieshammer, S.; Martin, M. Ab initio calculation of the attempt frequency of oxygen diffusion in pure and samarium doped ceria. *Phys. Chem. Chem. Phys.* **2017**, *19*, 9957−9973.
(37) Fan, G.; Wang, X.; Tu, X.; Xu, H.; Wang, Q.; Chu, X. Density functional theory study of Cu-doped BNNT as highly sensitive and selective gas sensor for carbon monoxide. *Nanotechnology* **2021**, *32*, No. 075502.
(38) Kaewmaraya, T.; Ngamwongwan, L.; Moontragoon, P.; Jarernboon, W.; Singh, D.; Ahuja, R.; Karton, A.; Hussain, T. Novel green phosphorene as a superior chemical gas sensing material. *J. Hazard. Mater.* **2021**, *401*, No. 123340.
(39) Koopmans, T. Ordering of wave functions and eigenenergies to the individual electrons of an atom. *Physica* **1934**, *1*, 104−113.
(40) Parr, R. G.; Szentpaly, L. V.; Liu, S. Electrophilicity index. *J. Am. Chem. Soc.* **1999**, *121*, 1922−1924.
(41) Lu, T.; Chen, F. Multiwfn: a multifunctional wavefunction analyzer. *J. Comput. Chem.* **2012**, *33*, 580−592.
(42) Bannwarth, C.; Ehlert, S.; Grimme, S. GFN2-xTB—An Accurate and Broadly Parameterized Self-Consistent Tight-Binding Quantum Chemical Method with Multipole Electrostatics and Density-Dependent Dispersion Contributions. *J. Chem. Theory Comput.* **2019**, *15*, 1652−1671.
(43) Pineda-Reyes, A. M.; Herrera-Rivera, M. R.; Rojas-Chávez, H.; Cruz-Martínez, H.; Medina, D. I. Recent Advances in ZnO-Based Carbon Monoxide Sensors: Role of Doping. *Sensors* **2021**, *21*, No. 4425.
(44) Cui, H.; Zhang, X.; Zhang, G.; Tang, J. Pd-doped MoS_2 monolayer: a promising candidate for DGA in transformer oil based on DFT method. *Appl. Surf. Sci.* **2019**, *470*, 1035−1042.
(45) Ma, S.; Li, D.; Rao, X.; Xia, X.; Su, Y.; Lu, Y. Pd-doped h-BN monolayer: a promising gas scavenger for SF_6 insulation devices. *Adsorption* **2020**, *26*, 619−626.
(46) Cui, H.; Jia, P.; Peng, X.; Li, P. Adsorption and sensing of CO and C_2H_2 by S-defected SnS_2 monolayer for DGA in transformer oil: A DFT study. *Mater. Chem. Phys.* **2020**, *249*, No. 123006.
(47) Zhao, Z.; Li, Z.; Wang, Q. Structures, electronic and magnetic properties of transition metal atoms encapsulated in $B_{12}N_{12}$ cage. *Chem. Phys. Lett.* **2020**, *739*, No. 136922.
(48) Vahed, S. A. $B_{12}N_{12}$ as a Sensor for the Detection of Nordazepam. *Med. Med. Chem.* **2024**, *1*, 14−19.
(49) Silva, A. L. P.; Silva, A. C. A.; Navis, C. N. N.; de Jesus Gomes Varela Júnior, J. Theoretical study of putrescine and $X_{12}Y_{12}$ (X = Al, B and Y = N, P) nanocage interactions. *J. Nanopart. Res.* **2021**, *23*, No. 108.
(50) Ahmadi, R. Furazolidone Adsorption on the Surface of $B_{12}N_{12}$: DFT Simulations. *J. Med. Med. Chem.* **2025**, *1*, 100−105.
(51) Mirderikvand, N.; Mahboubi-Rabbani, M. A DFT Study on Citalopram Adsorption on the Surface of $B_{12}N_{12}$. *Med. Med. Chem.* **2025**, *1*, 90−95.
(52) De Sousa Sousa, N.; Silva, A. L. P.; Silva, A. C. A.; de Jesus Gomes Varela Júnior, J. DFT Analysis of Structural, Energetic and Electronic Properties of Doped, Encapsulated, and Decorated First-Row Transition Metals on $B_{12}N_{12}$ Nanocage: Part 1. *J. Inorg. Organomet. Polym. Mater.* **2024**, *34*, 4082−4099.
(53) de Sousa Sousa, N.; da Conceição Lobato do Nascimento, W.; Silva, A. L. P.; de Jesus Gomes Varela Júnior, J. DFT study of TM (Sc-Zn) modified $B_{12}N_{12}$ nanocage as sensor for N_2O gas selective detection. *Sens. Actuators, A* **2024**, *378*, No. 115841.
(54) Parkar, P.; Mohammadi, M. D.; Chaudhari, A. Li-doped C_{20} nanocage and its derivatives for gas sensing application: A density functional theory study. *Talanta Open* **2025**, *11*, No. 100408.
(55) Nerkar, K. B.; Sonawane, M. R.; Chaudhari, A. Impact of LiTi and NaTi codecoration on hydrogen storage performance of C_{20} nanocage: A density functional theory study. *Chem. Phys. Lett.* **2026**, *883*, No. 142525.
(56) Ahangari, M. G.; Mashhadzadeh, A. H. Density functional theory based molecular dynamics study on hydrogen storage capacity of C_{24}, $B_{12}N_{12}$, Al_{12} N_{12}, $Be_{12}O_{12}$, $Mg_{12}O_{12}$, and $Zn_{12}O_{12}$ nanocages. *Int. J. Hydrogen Energy* **2020**, *45*, 6745−6756.
(57) Peng, S.; Cho, K.; Qi, P.; Dai, H. Ab initio study of CNT NO_2 gas sensor. *Chem. Phys. Lett.* **2004**, *387*, 271−276.
(58) Sergio, C. S.; Sousa, N. S. Theoretical investigation of H_2 adsorption on $B_{12}N_{12}$ nanocages decorated with Y, Zr, and Nb: stability, electronic properties and dynamic behavior. *Adsorption* **2025**, *31*, No. 109.
(59) Chakraborty, B.; Modak, P.; Banerjee, S. Hydrogen Storage in Yttrium-Decorated Single Walled Carbon Nanotube. *J. Phys. Chem. C* **2012**, *116*, 22502−22508.
(60) Paul, D.; Mane, P.; Sarkar, U.; Chakraborty, B. Yttrium decorated fullerene C_{30} as potential hydrogen storage material: Perspectives from DFT simulations. *Theor. Chem. Acc.* **2023**, *142*, No. 94.
(61) Rad, A. S.; Ayub, K. Ni adsorption on $Al_{12}P_{12}$ nano-cage: a DFT study. *J. Alloys Compd.* **2016**, *678*, 317−324.
(62) Escobedo-Morales, A.; Tepech-Carrillo, L.; Bautista-Hernández, A.; Camacho-García, J. G.; Cortes-Arriagada, D.; Chigo-Anota, E. Effect of Chemical Order in the Structural Stability and Physicochemical Properties of $B_{12}N_{12}$ Fullerenes. *Sci. Rep.* **2019**, *9*, No. 16521.
(63) Silva, A. L. P.; de Jesus Gomes Varela Júnior, J. Carbon monoxide interaction with $B_{12}N_{12}$ nanocage with and without an external electric field: a DFT study. *J. Nanopart. Research* **2022**, *24*, No. 1.
(64) Costa, A. M. F.; Silva, T. S.; Oh, L. B. C.; Pereira, D. H. Interaction of Fe^{2+}, Co^{2+}, Ni^{2+}, Cu^{2+}, Zn^{2+}, Pb^{2+}, and Cr^{3+} metal ions on $B_{12}N_{12}$ fullerene-like cages: a theoretical study. *Monatsh. Chem.* **2021**, *152*, 915−922.
(65) Pearson, R. G. The principle of maximum hardness. *Acc. Chem. Res.* **1993**, *26*, 250−255.
(66) Pearson, R. G. Absolute electronegativity and hardness correlated with molecular orbital theory. *Proc. Natl. Acad. Sci. U.S.A.* **1986**, *83*, 8440−8441.
(67) Hizaddin, H. F.; Hashim, M. A.; Anantharaj, R. Evaluation of molecular interaction in binary mixture of ionic Liquids+ heterocyclic

https://doi.org/10.1021/acsomega.5c11273
ACS Omega XXXX, XXX, XXX−XXX

nitrogen compounds: ab Initio method and COSMO-RS model. *Ind. Eng. Chem. Res.* **2013**, *52*, 18043−18058.
(68) Makhlouf, J.; Louis, H.; Benjamin, I.; Ukwenya, E.; Valkonen, A.; Smirani, W. Single crystal investigations, spectral analysis, DFT studies, antioxidants, and molecular docking investigations of novel hexaiso-thiocyanato chromate complex. *J. Mol. Struct.* **2023**, *1272*, No. 134223.
(69) Alabugin, I. V.; Manoharan, M.; Peabody, S.; Weinhold, F. Electronic basis of improper hydrogen bonding: a subtle balance of hyperconjugation and rehybridization. *J. Am. Chem. Soc.* **2003**, *125*, 5973−5987.
(70) Bader, R. F. W. Atoms in molecules. *Acc. Chem. Res.* **1985**, *18*, 9−15.
(71) Janjua, M. R. S. A. Theoretical Framework for Encapsulation of Inorganic $B_{12}N_{12}$ Nanoclusters with Alkaline Earth Metals for Efficient Hydrogen Adsorption: A Step Forward toward Hydrogen Storage Materials. *Inorg. Chem.* **2021**, *60*, 2816−2828.
(72) De Sousa Sousa, N.; Silva, A. L. P.; Silva, A. C. A.; de Jesus Gomes Varela Júnior, J. DFT Analysis of Dynamic, Charge, and TD-DFT Properties of Doped, Encapsulated, and Decorated First-Row Transition Metals on $B_{12}N_{12}$ Nanocage: Part 2. *J. Inorg. Organomet. Polym. Mater.* **2024**, *34*, 3576−3588.
(73) Angizi, S.; Shayeganfarc, F.; Azara, M. H.; Simchia, A. Surface/edge functionalized boron nitride quantum dots: Spectroscopic fingerprint of bandgap modification by chemical functionalization. *Ceram. Int.* **2020**, *46*, 978−985.
(74) Wang, X.; Chertihin, G. V.; Andrews, L. Matrix Infrared Spectra and DFT Calculations of the Reactive MH_x (x = 1, 2, and 3), (H_2) MH_2, MH_2^+, and MH_4^- (M= Sc, Y, and La) Species. *J. Phys. Chem. A* **2002**, *106*, 9213−9225.
(75) Nair, L.; Sankar, J.; Nair, S. A.; Kumar, G. V. Biological Evaluation of 5-Fluorouracil Nanoparticles for Cancer Chemotherapy and Its Dependence on the Carrier, PLGA. *Int. J. Nanomed.* **2011**, *6*, 1685−1697.
(76) Taherpour, A. A.; Shahri, Z.; Rezaei, O.; Jamshidi, M.; Fellowes, T. Adsorption, intercalation and sensing of helium on yttrium functionalized open edge boron nitride: A first principle DFT and TDDFT study. *Chem. Phys. Lett.* **2018**, *691*, 231−237.
(77) Mondal, B.; Basumatari, B.; Das, J.; Roychaudhury, C.; Saha, H.; Mukherjee, N. ZnO−SnO_2 based composite type gas sensor for selective hydrogen sensing. *Sens. Actuators, B* **2014**, *194*, 389−396.
(78) Umar, A.; Ammar, H. Y.; Kumar, R.; Almas, T.; Ibrahim, A. A.; Al Assiri, M. S.; Abaker, M.; Baskoutas, S. Efficient H_2 gas sensor based on 2D SnO_2 disks: experimental and theoretical studies. *Int. J. Hydrogen Energy* **2020**, *45*, 26388−26401.
(79) Ghamsari, P. A.; Nouraliei, M.; Gorgani, S. S. DFT simulation towards evaluation the molecular structure and properties of the heterogeneous $C_{16}Mg_8O_8$ nano-cage as selective nano-sensor for H_2 and N_2 gases. *J. Mol. Graphics Modell.* **2016**, *70*, 163−169.
(80) Pal, P.; Yadav, A.; Chauhan, P. S.; Parida, P. K.; Gupta, A. Reduced graphene oxide based hybrid functionalized films for hydrogen detection: Theoretical and experimental studies. *Sens. Int.* **2021**, *2*, No. 100072.
(81) Yang, S.; Xie, S.; Tan, L.; Lei, G.; Xu, H.; Lan, Z.; Wang, Z.; Gu, H. Selective and tunable H_2 adsorption/sensing performance of W-doped graphene under external electric fields: A DFT study. *Int. J. Hydrogen Energy* **2022**, *47*, 29579−29591.
(82) Zakeri, S. S.; Rouhani, M.; Mirjafary, Z. Comparative DFT study on the H_2 adsorption and the sensing properties of BN-, BP-, AlN-, and AlP-decorated graphene nanoflakes. *Diamond Relat. Mater.* **2020**, *130*, No. 109510.
(83) Luo, S.; Zhou, Q.; Xue, W.; Liao, N. Effect of Pt doping on sensing performance of g-C_3N_4 for detecting hydrogen gas: a DFT study. *Vacuum* **2022**, *200*, No. 111014.
(84) Li, F.; Asad, H. DFT study of the effect of platinum on the H_2 gas sensing performance of ZnO nanotube: Explaining the experimental observations. *J. Mol. Liq.* **2020**, *309*, No. 113139.
(85) Li, T.; Yin, H.; Yang, S.; Lei, G.; Wang, Z.; Xu, H.; Gu, H. WS_2 monolayer decorated with single-atom Pt for outstanding H_2 adsorption and sensing: A DFT study. *Int. J. Hydrogen Energy* **2025**, *141*, 1078−1087.
(86) Jiang, T.; Zhang, W.; Zhang, T.; Yuan, H.; Bi, M.; Zhou, X. Adsorption and gas-sensing performances of C_2H_2, C_2H_4, CO, H_2 in transformer oil on Pt-doped $MoTe_2$ monolayer: A DFT study. *Phys. E* **2023**, *146*, No. 115568.
(87) Imeni, S.; Rouhani, M.; Aliabad, J. M. NiN_4S-doped single walled carbon nanotube as an ultrafast H_2 gas sensor: A DFT simulation. *Inorg. Chem. Commun.* **2023**, *148*, No. 110334.
(88) Huang, B.; Li, L.; Ma, Y.; Xie, W.; Li, K. Research on $Al_{12}C_{12}$ as a gas sensor for detecting of CH_4, CO, H_2, NO and NH_3 based on density functional theory. *J. Nanopart. Res.* **2025**, *27*, No. 48.

https://doi.org/10.1021/acsomega.5c11273
ACS Omega XXXX, XXX, XXX−XXX